




Energy Budgets for Terrestrial Extrasolar Planets

Aomawa L. Shields¹ , Cecilia M. Bitz², and Igor Palubski¹¹ Department of Physics and Astronomy University of California, Irvine, 4129 Frederick Reines Hall Irvine, CA 92697-4575, USA; shields@uci.edu² Department of Atmospheric Sciences, University of Washington, Seattle, WA 98105-6698, USA

Received 2019 August 16; revised 2019 September 11; accepted 2019 September 14; published 2019 October 3

Abstract

The pathways through which incoming energy is distributed between the surface and atmosphere have been analyzed for the Earth. However, the effect of the spectral energy distribution of a host star on the energy budget of an orbiting planet may be significant given the wavelength-dependent absorption properties of atmospheric CO₂, water vapor, surface ice, and snow. We have quantified the flow of energy on aqua planets orbiting M-, G-, and F-dwarf stars, using a 3D Global Climate Model with a static ocean. The atmosphere and surface of an M-dwarf planet receiving an instellation equal to 88% of the modern solar constant at the top of the atmosphere absorb 12% more incoming stellar radiation than those of a G-dwarf planet receiving 100% of the modern solar constant, and 17% more radiation than an F-dwarf planet receiving 108% of the modern solar constant, resulting in climates similar to that of modern-day Earth on all three planets, assuming a 24 hr rotation period and fixed CO₂. At 100% instellation, a synchronously rotating M-dwarf planet exhibits smaller flux absorption in the atmosphere and on the surface of the dayside, and a dayside mean surface temperature that is 37 K colder than its rapidly rotating counterpart. Energy budget diagrams are included to illustrate the variations in global energy budgets as a function of host star spectral class, and can contribute to habitability assessments of planets as they are discovered.

Unified Astronomy Thesaurus concepts: [Astrobiology \(74\)](#); [Interdisciplinary astronomy \(804\)](#); [Exoplanets \(498\)](#); [Habitable planets \(695\)](#); [Exoplanet surface composition \(2022\)](#); [Exoplanet atmospheric composition \(2021\)](#)

1. Introduction

A planet's climate is largely determined by its global energy balance between the incoming stellar (shortwave) radiation and the outgoing thermal (longwave) radiation emitted to space. This delicate balance is achieved through a combination of reflected, absorbed, and/or emitted shortwave (SW) and longwave radiation throughout a planet's atmosphere and surface. The global energy budget of the Earth has been calculated, based on both numerical simulations and direct observations, and its partitioning is often depicted graphically in what is known as a "Trenberth diagram" (Kiehl & Trenberth 1997; Fasullo & Trenberth 2008; Trenberth et al. 2009; Stephens et al. 2012). Analyses of Earth's energy budget have led to a deeper understanding of the various pathways through which incoming energy from a host star flows and is cycled by a planet's atmosphere and surface. Such analyses have been used to identify sources of imbalance in the Earth's system, such as that which currently exists as a result of anthropogenic CO₂ emissions (Hansen et al. 2005, 2011; Trenberth et al. 2014). Trenberth diagrams have also been calculated for Venus, Mars, Jupiter, Titan, and the "hot Jupiter" exoplanet HD 189733b (Read et al. 2016).

The interaction between the spectral energy distribution (SED) of a host star and the atmospheres and surfaces of orbiting planets has been shown to strongly affect planetary climate, and these effects depend on the amount of flux emitted by stars in certain wavelength regions (Shields et al. 2013, 2014; von Paris et al. 2013; Godolt et al. 2015; Wolf et al. 2017; Shields & Carns 2018). Given the wavelength-dependent absorption properties of atmospheric gases as well as surface types, the interaction between host star SED and a planet's atmosphere and surface will therefore

influence the various pathways and associated energy budgets of orbiting planets, and the manner in which global energy balance is attained. The atmospheres and icy surfaces of planets orbiting M-dwarf stars have been found to absorb more radiation overall than those of their counterparts orbiting stars with more visible and UV output at equivalent stellar flux distances and with equal rotation periods, resulting in warmer surface temperatures and greater climate stability on M-dwarf planets (Shields et al. 2013, 2014). However, the amount of radiation absorbed versus reflected, and other components of the energy budget on an orbiting planet as a function of its host star's SED, has not been quantified, yet the energy budget controls how the surface temperature and climate will evolve over time for planets in different stellar environments.

In this work we have simulated the climates of planets orbiting M-, G-, and F-dwarf stars, and calculated energy budgets that track the flow of SW and longwave radiation throughout each planet. We provide these energy budgets in the form of schematic diagrams. We identified the amount of stellar radiation incoming at the top of the atmosphere (hereafter "instellation") necessary to yield global mean surface temperatures approximating that of modern-day Earth as a function of host star spectral type, and compared the energy budgets for these planets to isolate the effect of stellar SED on their pathways to similar climates.

Planets orbiting close to their stars will experience strong tidal effects, potentially resulting in captures into spin-orbit resonances (Dole 1964) such as a 1:1 spin-orbit resonance, where the substellar point of the planet is fixed with time (synchronous rotation). Such a state will significantly impact a planet's climate (Joshi et al. 1997; Merlis & Schneider 2010; Edson et al. 2011; Showman et al. 2010, 2013; Showman & Polvani 2011; Heng & Kopparla 2012; Yang et al. 2014; Kaspi & Showman 2015). We also simulated the climate of a synchronously rotating M-dwarf planet receiving 100% of the modern solar constant to examine the effects of this extreme



Original content from this work may be used under the terms of the [Creative Commons Attribution 3.0 licence](#). Any further distribution of this work must maintain attribution to the author(s) and the title of the work, journal citation and DOI.

rotational state on global energy budgets and pathways compared with its rapidly rotating counterpart.

In Section 2 we describe the model and methods used to simulate the climates of planets orbiting stars of different spectral types. We present results from these simulations, including Trenberth diagrams and a table of energy budgets, in Section 3. An analysis and discussion of the differences in energy budgets for the planets explored is provided in Section 4. Conclusions follow in Section 5.

2. Methods and Models

We used version 4 of the Community Climate System Model (CCSM4), a three-dimensional (3D) global climate model (GCM) developed to simulate and predict climate and weather patterns on the Earth (Gent et al. 2011). CCSM4 contains an atmospheric component (The Community Atmosphere Model version 4, or CAM4) and the Los Alamos sea-ice model (CICE version 4; Hunke & Lipscomb 2008). We ran simulations with a 50 m deep slab ocean without heat flux, but treated as fully mixed with depth. This suite of coupled model components has been used in previous work (see, e.g., Bitz et al. 2012; Shields et al. 2013, 2014, 2016; Shields & Carns 2018). The horizontal angular resolution is nominally 2° . We modified the percentages of incoming stellar flux in each of the 12 wavelength bands that are input to CAM4 according to the SEDs of G2V star The Sun (Chance & Kurucz 2010), M3V star AD Leo³ (Reid et al. 1995; Segura et al. 2005), and F2V star HD 128167⁴ (Segura et al. 2003). For full details on how the model has been applied to exoplanets, see Shields et al. (2013).

We simulated the climates of M-, G-, and F-dwarf aqua planets (no land) receiving a range of instellations from their host stars, assuming circular orbits, a radius, mass, and obliquity equal to the Earth's, and atmospheres with 1 bar surface pressure and Earth-like levels of CO₂. Water vapor was permitted to adjust during each simulation in accordance with standard evaporation and precipitation processes on the surface and in the atmosphere. We simulated Earth-like (24 hr) rotation periods and also a synchronous rotation period (obliquity = 0) for the M-dwarf planet. We identified the level of instellation required from M- and F-dwarf host stars to generate climates similar to that of modern-day Earth.

As done in Shields et al. (2013, 2014, 2016) and Shields & Carns (2018), we used the sea-ice albedo parameterization of CCSM3, as it is easier to manipulate than later versions. This parameterization divides the surface albedo into two bands, visible ($\lambda \leq 0.7 \mu\text{m}$) and near-IR ($\lambda > 0.7 \mu\text{m}$). The default near-IR and visible band albedos, tuned for a solar spectrum, are 0.30 and 0.67 for cold bare ice, and 0.68 and 0.80 for cold dry snow, respectively. For our simulations of M- and F-dwarf planet climates, we calculated the two-band albedos weighted by the spectrum of each host star. All ice and snow albedos used are provided in Table 1. We present a comparison and analysis of the differences in the planets' global energy budgets in the following sections.

3. Results

Figure 1 shows the global mean surface temperature for planets receiving different amounts of instellation from M-, G-, and F-dwarf stars, and annual mean energy budget values for planets receiving the amount of instellation to yield equivalent,

Table 1

Two-band Albedos Employed for Ice and Snow in the GCM, Weighted by the Spectrum for G-dwarf Star the Sun, M-dwarf Star AD Leo, and F-dwarf Star HD 128167

Host star	$T < 0^\circ\text{C}$	$E - P < 0$
Band	NIR/VIS	NIR/VIS
M-dwarf	0.18/0.69	0.49/0.97
G-dwarf	0.30/0.67	0.68/0.80
F-dwarf	0.27/0.73	0.67/0.99

Note. E and P denote water evaporation and precipitation, respectively.

(modern-day) Earth-like climates. The F-dwarf planet required 108% of the modern solar constant to generate a global mean surface temperature of 287 K, similar to that of modern-day Earth and to that of the G-dwarf planet receiving 100% of the modern solar constant (288 K). The M-dwarf planet required only 88% of the modern solar constant to produce a similar climate, with a global mean surface temperature of 287 K (Figure 1(a)).

While the F-dwarf planet receives the largest amount of instellation from its host star, its atmosphere also reflects the largest percentage of that incoming instellation—2% more than the G-dwarf planets' atmosphere (Figure 1(b)) and nearly 12% more than the M-dwarf planet's atmosphere—while the M-dwarf planet's atmosphere absorbs the most—over 15% more than the G-dwarf's, and nearly 20% more than the F-dwarf's (Figure 1(c)). At the surface, the F-dwarf planet also reflects the largest percentage of its incoming radiation, 16% of the SW that reaches the surface, 5% and 9% more than the surfaces of the G- and M-dwarf planets, respectively. In contrast, the M-dwarf planet absorbs the most—93%—of the SW reaching the surface (Figure 1(d)), $\sim 4\%$ more than the G-dwarf planet's surface and 9% more than the surface of the F-dwarf planet. The M-dwarf planet, whose atmosphere and surface combined absorb 12% more radiation than the G-dwarf planet and 17% more radiation than the F-dwarf planet, has a correspondingly larger outgoing longwave radiation (OLR). Energy budget fluxes for all three planets are shown in Table 2.

Figure 2 shows annually averaged climatic variables across the three planets, all of which have open water in the tropics and mid latitudes. At higher latitudes where there is ice on these planets, the F-dwarf planet has the highest surface albedos (Figure 2(a)), while the M-dwarf planet has the lowest, with a lower ice fraction in these regions (Figure 2(b)). Surface temperatures are warmer here on the M-dwarf planet (Figure 2(c)). The higher instellation received by the F-dwarf increases the specific humidity in the tropics and mid latitudes where there is open ocean to absorb strongly (Figure 2(d)), resulting in slightly warmer temperatures here relative to the other two planets. However, in the high-latitude ice-covered regions the larger absorption of radiation by lower-albedo ice on the M-dwarf planet increases the specific humidity by a larger factor relative to the F-dwarf planet, contributing to significantly increased surface temperatures at higher latitudes and a smaller equator-to-pole temperature contrast on the M-dwarf planet compared to the F- and G-dwarf planets.

Figure 3 shows the annual mean energy budget for an M-dwarf planet with a 24 hr rotation period receiving 100% of the modern solar constant from its star, the dayside of a synchronously rotating M-dwarf planet receiving equivalent instellation, and a contour map of the annual mean surface

³ <http://vpl.astro.washington.edu/spectra/stellar/mstar.htm>

⁴ http://vpl.astro.washington.edu/spectra/stellar/other_stars.htm

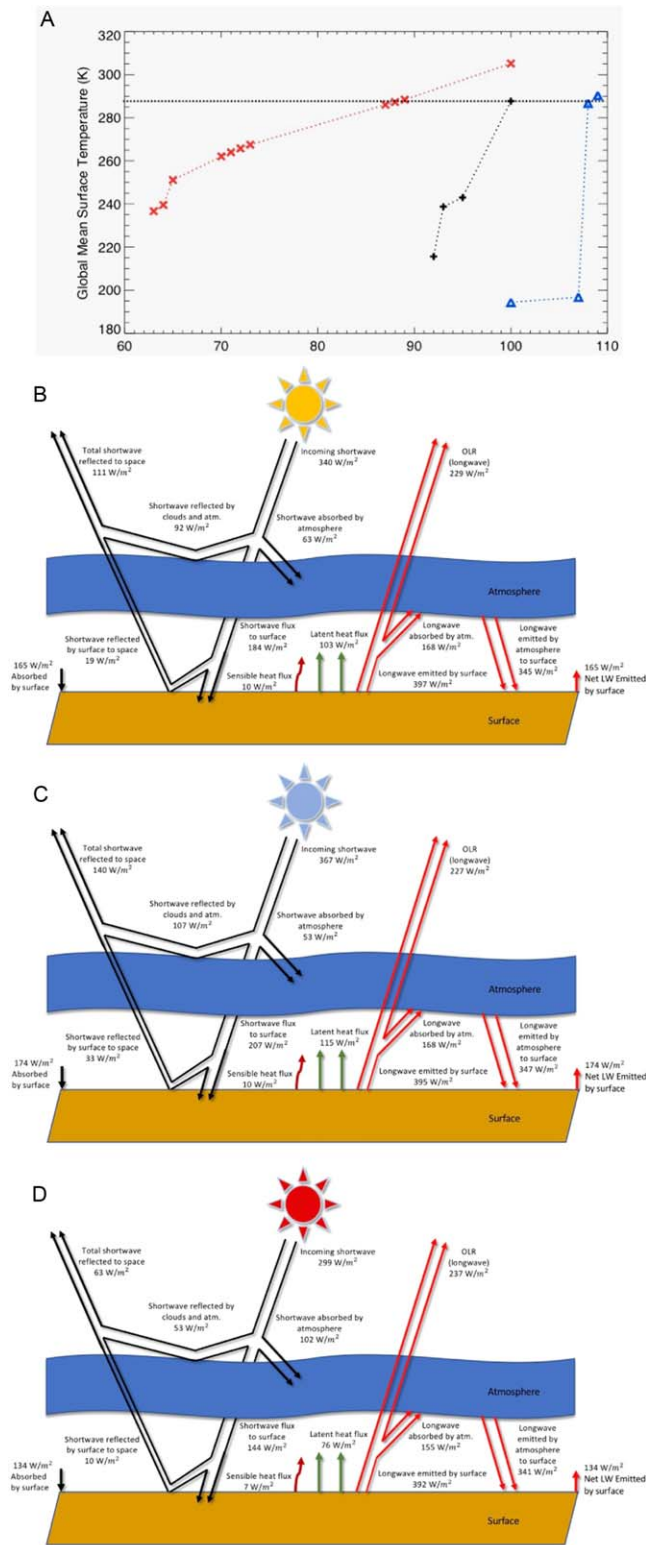


Figure 1. Top row: global mean surface temperature as a function of instellation for F- (blue triangles), G- (black plus symbols), and M-dwarf (red x's) terrestrial planets, averaged over 60–120 yr of CCSM simulations. The horizontal black dotted line indicates a temperature of ~ 288 K, similar to that of modern-day Earth, and aligns closest to the G-dwarf planet at 100% instellation (second row), the F-dwarf planet receiving 108% instellation (third row), and the M-dwarf planet at 88% instellation (fourth row), whose annual mean global energy budgets at the top of the atmosphere and the surface are averaged over 80–100 yr of CCSM simulations.

Table 2

Selected Annual Mean Radiative Fluxes (in $W m^{-2}$) for Planets Receiving the Instellation Necessary from F-, G-, and M-dwarf Host Stars to Yield Global Mean Surface Temperatures Similar to that of Modern-day Earth

	Flux	F-dwarf	G-dwarf	M-dwarf
	Global mean surface temperature (K)	287	288	287
	Instellation (percent of the modern solar constant)	108	100	88
SW	Incoming	367	340	299
	Reflected by atmosphere	107	92.2	52.7
	Percentage of incoming SW	29.2%	27.1%	17.6%
	Absorbed by atmosphere	52.9	63.3	102
	Percentage of incoming SW	14.4%	18.6%	34.2%
	Reaching surface	207	184	144
	Reflected (surface)	33.0	19.2	9.78
	Percentage of SW reaching surface	15.9%	10.4%	6.79%
	Absorbed (surface)	174	165	134
	Percentage of SW reaching surface	84.1%	89.6%	93.2%
LW	Emitted by surface	395	397	392
	Absorbed by atmosphere	168	168	155
	Percentage of emitted by surface	42.4%	42.3%	39.6%
	Emitted by atmosphere to surface	347	345	341
	OLR	227	229	237
	Percentage of emitted by surface	57.5%	57.6%	60.4%

Note. SW is incoming stellar radiative flux. LW is outgoing thermal flux from the planet. An obliquity of 23° and a 24 hr rotation period is assumed for all three planets.

temperature across the synchronous planet. Of the $680 W m^{-2}$ received by the dayside of the synchronous planet ($1360 W m^{-2}$ divided by 2), 26% is reflected by the atmosphere and 38% is absorbed, compared with 15% reflected and 43% absorbed by that of the M-dwarf planet with a 24 hr rotation period (Figure 3(a)). While a similar percentage of each planet's incoming SW reaches the surface, 56% less flux is absorbed by the dayside surface of the synchronously rotating planet (Figure 3(b)). However, of the SW absorbed by the entire dayside (atmosphere + surface), only 53% leaves as OLR. This lower relative thermal emission results in dayside surface temperatures reaching 287 K, and a sizable region above freezing (>273 K) at the substellar point. Temperatures do get 66° colder (221 K) on portions of the dayside of the planet (Figure 3(c)), resulting in ice cover in those annuli. Though this ice present on the dayside has a relatively low albedo, it is still more reflective than ocean, which comprises the entire surface of the rapidly rotating planet, which never gets below freezing. The dayside mean surface temperature is ~ 268 K, 37° colder than the rapidly rotating M-dwarf planet (305 K), which has a narrower temperature difference (42 K) between maximum (319 K) and minimum (277 K) surface temperatures. The nightside of the planet gets as cold as 218 K, resulting in a global mean surface temperature of 245 K on the synchronously rotating M-dwarf planet, 60° colder than its rapidly rotating counterpart.

4. Discussion

Our results indicate that a host star's spectral type has a significant effect on the energy budget of an orbiting terrestrial

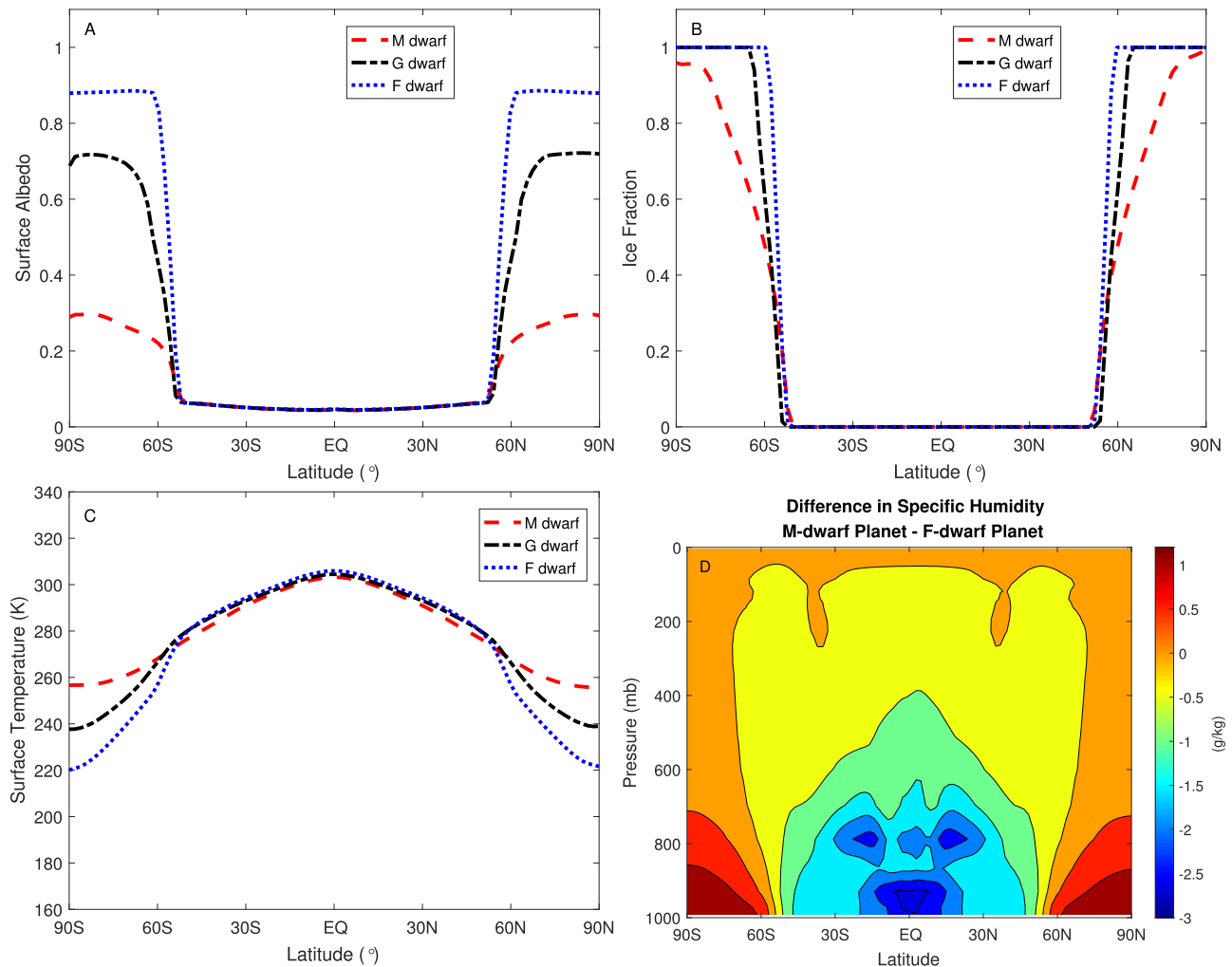


Figure 2. Annual mean surface albedo, ice fraction, surface temperature, and specific humidity (M-dwarf planet minus F-dwarf planet) for F-, G-, and M-dwarf planets with climates similar to that of modern-day Earth and receiving 108%, 100%, and 88% of the modern solar constant from their host stars, averaged over 60–100 yr of CCSM simulations.

planet, assuming fixed CO_2 levels and equivalent planetary rotation periods. The interactions between host star SED and gases such as CO_2 and H_2O in a planet’s atmosphere, and icy and snowy surfaces on the ground, all of which have wavelength-dependent absorption properties, are responsible for the difference in energy budgets for planets orbiting different types of stars. Each star–planet interaction produces a unique partitioning of the incoming SW and outgoing LW, resulting in a specific pathway to a planet’s climate that varies with host star spectral type. The spectrum dependence of the energy budgets of terrestrial planets, when quantified, reveals that the increased absorption of incoming near-IR radiation by the atmospheres and surfaces of M-dwarf planets causes these planets to be warmer than planets orbiting hotter, brighter stars at equivalent flux distances and require less instellation to produce similar climates, assuming similar planetary rotation periods and atmospheric gas concentrations.

The amount of instellation required to generate a climate similar to that of modern-day Earth varies with host star spectral type. The atmosphere and surface of a planet orbiting an F-dwarf star reflect more incoming radiation than those of a G- or M-dwarf planet, requiring 8% and 20% more incoming radiation to produce a climate similar to these planets, respectively. The higher albedo of water ice in the visible

and near-UV, where the F-dwarf star strongly emits, combined with the reduced atmospheric absorption on this planet, as CO_2 and water vapor absorb strongly in the near-IR rather than the visible or near-UV, cause the F-dwarf planet to require more incoming stellar radiation to raise its global mean surface temperature to a level on par with the G-dwarf planet. In contrast, the M-dwarf planet’s atmosphere and surface absorb more radiation, resulting in a smaller instellation required to yield a similar climate to the G-dwarf planet—only 88% of the modern solar constant, assuming a 24 hr rotation period for all planets.

Previous work determined that the instellation value required for global ice cover on an F-dwarf planet was 98% of the modern solar constant, while an M-dwarf planet was found to require 90% of the modern solar constant from its star to exhibit a climate similar to that of modern-day Earth (Shields et al. 2013, 2014). The higher instellation value for a frozen F-dwarf planet (107% instellation, shown in Figure 1(a)) and lower value for Earth-like conditions on the M-dwarf planet in this work are due to the weighting of the water ice and snow albedos by the spectra of our host stars here, yielding lower near-IR and higher visible ice and snow albedos for M- and F-dwarf spectra, respectively—rather than using the default albedo parameterization in the GCM.

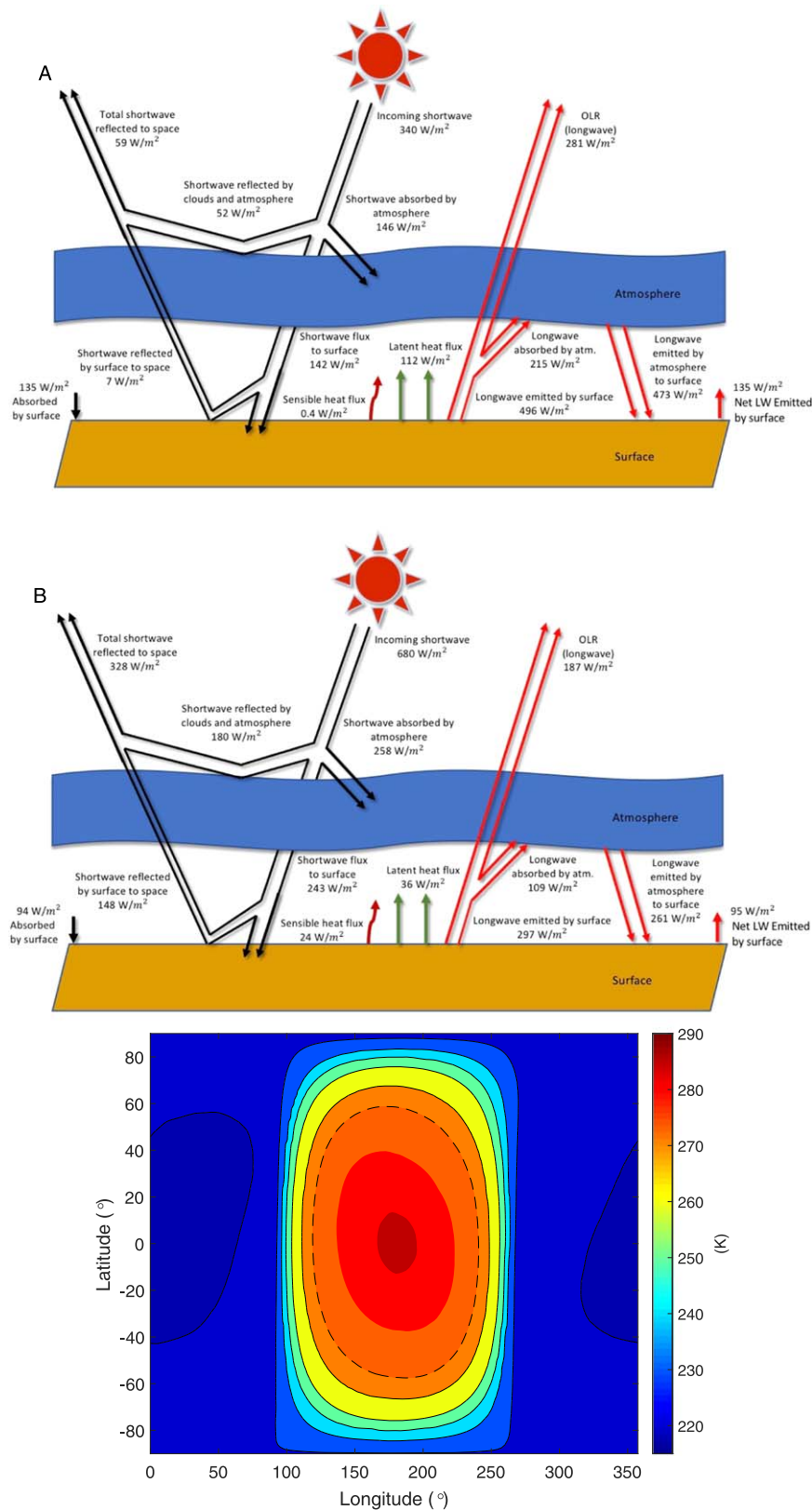


Figure 3. Top: annual mean energy budgets for a terrestrial M-dwarf planet with a 24 hr rotation period receiving 100% of the modern solar constant from its host star, averaged over 80 yr of CCSM simulations. Middle: annual mean energy budgets for a synchronously rotating M-dwarf planet receiving equivalent instellation. Bottom: surface temperature as a function of latitude and longitude for the synchronously rotating planet. Zero eccentricity and obliquity are assumed for the synchronous planet. The freezing point (273 K) on the planet is labeled by a dashed contour line.

A fixed substellar point and lower relative thermal emission on the synchronously rotating M-dwarf planet keeps temperatures warm on the dayside. However, the planet exhibits a

lower maximum dayside surface temperature than the global mean surface temperature of the rapidly rotating planet. Previous work found that weakened low-latitude zonal winds

cool synchronously rotating planets (Edson et al. 2011), which have been shown to exhibit lower dayside minimum surface temperatures than those on rapidly rotating planets (Shields & Carns 2018). These differences, as well as a greater amount of cloud cover at the substellar point, which has been shown to cool synchronously rotating planets (Yang et al. 2013), contribute to the resulting energy budget of this planet, with a smaller percentage of its incoming radiation absorbed both in the atmosphere and at the surface compared to the rapidly rotating case, cooling temperatures.

We held the atmospheric CO₂ concentration fixed in all of our simulations, to isolate the effect of host star SED on a planet's global energy budget. The existence of an active carbon cycle on exoplanets is uncertain, and would certainly affect the energy budgets. If such a cycle operates as it does on the Earth, where the silicate weathering rate is adjusted with temperature (see, e.g., Walker et al. 1981), it can be expected that the stronger radiative response to increases in CO₂ for M-dwarf planets (see, e.g., Shields et al. 2013) may lead to increased fluxes within their absorption budget pathways farther out in their stars' habitable zones compared to G- and F-dwarf planets receiving equivalent instellation. However, the increased instellation required to produce similar climates on G- and F-dwarf planets may help to match any amplified radiative response to increases in CO₂ on M-dwarf planets.

5. Conclusions

Using a 3D GCM to calculate energy budget “Trenberth” diagrams for planets orbiting F-, G-, and M-dwarf stars, we have shown that the SED of a host star heavily influences the energy budget of an orbiting planet. An M-dwarf planet requires 12% less instellation than a G-dwarf planet to exhibit a climate similar to that of modern-day Earth, while an F-dwarf planet requires 8% more instellation, assuming a 24 hr rotation period and fixed CO₂. The atmosphere and surface of the M-dwarf planet absorb 12% more incoming flux than a G-dwarf planet and 17% more flux than the F-dwarf planet, compensating for the reduced instellation. The spectral dependence of ice and snow albedo, with both absorbing strongly in the near-IR where M dwarfs emit strongly, while heavily reflecting in the visible and near-UV where brighter stars emit, along with CO₂ and H₂O in the atmosphere absorbing mainly in the near-IR, are responsible for this difference in energy budgets and resulting instellation requirements for planets orbiting different types of stars. For synchronously rotating M-dwarf planets, smaller flux absorption in the atmosphere and on the surface results in lower minimum/maximum dayside surface temperatures compared to those on M-dwarf planets with 24 hr rotation periods receiving equivalent instellation, with a dayside mean surface temperature that is 37 K colder than its rapidly rotating counterpart. Should an active carbon cycle exist on exoplanets, the stronger radiative response to increases in CO₂ for M-dwarf planets may be matched by the increased instellation required to generate equivalent climates on planets orbiting stars with more visible and near-UV output.

This material is based upon work supported by NASA under grant No. NNH16ZDA001N, which is part of the “Habitable

Worlds” program, by the National Science Foundation under Award 1753373, and by a Clare Boothe Luce Professorship supported by the Henry Luce Foundation. This research was also supported in part by the National Science Foundation under grant No. NSF PHY-1748958, and was performed as part of the NASA Astrobiology Institute's Virtual Planetary Laboratory under Cooperative Agreement Number NNA13AA93A. We would like to acknowledge high-performance computing support from Cheyenne (doi:10.5065/D6RX99HX) provided by NCAR's Computational and Information Systems Laboratory, sponsored by the National Science Foundation. We thank Kevin Trenberth and John Fasullo for providing guidance on calculating specific energy budget values from numerical simulations. We also thank Dorian Abbot for reading earlier versions of this manuscript and providing helpful feedback.

ORCID iDs

Aomawa L. Shields  <https://orcid.org/0000-0002-7086-9516>

References

- Bitz, C. M., Shell, K. M., Gent, P. R., et al. 2012, *JCLI*, **25**, 3053
 Chance, K., & Kurucz, R. L. 2010, *JQSRT*, **111**, 1289
 Dole, S. H. 1964, *Habitable Planets for Man* (New York: Blaisdell)
 Edson, A., Lee, S., Bannon, P., Kasting, J. F., & Pollard, D. 2011, *Icar*, **212**, 1
 Fasullo, J. T., & Trenberth, K. E. 2008, *JCLI*, **21**, 2297
 Gent, P. R., Danabasoglu, G., Donner, L. J., et al. 2011, *JCLI*, **24**, 4973
 Godolt, M., Grenfell, J. L., Hamann-Reinus, A., et al. 2015, *P&SS*, **111**, 62
 Hansen, J., Nazarenko, L., Ruedy, R., et al. 2005, *Sci*, **308**, 1431
 Hansen, J., Sato, M., Kharecha, P., & von Schuckmann, K. 2011, *ACP*, **11**, 13421
 Heng, K., & Kopparla, P. 2012, *ApJ*, **754**, 60
 Hunke, E. C., & Lipscomb, W. H. 2008, CICE: The Los Alamos Sea Ice Model. Documentation and Software User's Manual, Tech. Rep. LA-CC-06-012, Version 4.0. (T-3 Fluid Dynamics Group, Los Alamos National Laboratory)
 Joshi, M. M., Haberle, R. M., & Reynolds, R. T. 1997, *Icar*, **129**, 450
 Kaspi, Y., & Showman, A. P. 2015, *ApJ*, **804**, 60
 Kiehl, J. T., & Trenberth, K. E. 1997, *BAMS*, **78**, 197
 Merlis, T. M., & Schneider, T. 2010, *JAMES*, **2**, 13
 Read, P. L., Barstow, J., Charnay, B., et al. 2016, *QJRM*, **142**, 703
 Reid, I. N., Hawley, S. L., & Gizis, J. E. 1995, *AJ*, **110**, 1838
 Segura, A., Kasting, J. F., Meadows, V., et al. 2005, *AsBio*, **5**, 706
 Segura, A., Krellove, K., Kasting, J. F., et al. 2003, *AsBio*, **3**, 689
 Shields, A. L., Barnes, R., Agol, E., et al. 2016, *AsBio*, **16**, 443
 Shields, A. L., Bitz, C. M., Meadows, V. S., Joshi, M. M., & Robinson, T. D. 2014, *ApJL*, **785**, L9
 Shields, A. L., & Carns, R. C. 2018, *ApJ*, **867**, 11
 Shields, A. L., Meadows, V. S., Bitz, C. M., et al. 2013, *AsBio*, **13**, 715
 Showman, A. P., Cho, J. Y.-K., & Menou, K. 2010, in *Exoplanets*, ed. S. Seager (Tucson, AZ: Univ. Arizona Press), 471
 Showman, A. P., & Polvani, L. M. 2011, *ApJ*, **738**, 71
 Showman, A. P., Wordsworth, R. D., Merlis, T. M., & Kaspi, Y. 2013, in *Atmospheric Circulation of Terrestrial Exoplanets*, ed. S. J. Mackwell et al., 277
 Stephens, G. L., Li, J., Wild, M., et al. 2012, *NatGe*, **5**, 691
 Trenberth, K. E., Fasullo, J. T., & Balmaseda, M. A. 2014, *JCLI*, **27**, 3129
 Trenberth, K. E., Fasullo, J. T., & Kiehl, J. 2009, *BAMS*, **90**, 311
 von Paris, P., Selsis, F., Kitzmann, D., & Rauer, H. 2013, *AsBio*, **13**, 899
 Walker, J. C. G., Hays, P. B., & Kasting, J. F. 1981, *JGR*, **86**, 9776
 Wolf, E. T., Shields, A. L., Kopparapu, R. K., Haqq-Misra, J., & Toon, O. B. 2017, *ApJ*, **837**, 107
 Yang, J., Boué, G., Fabrycky, D. C., & Abbot, D. S. 2014, *ApJL*, **787**, L2
 Yang, J., Cowan, N. B., & Abbot, D. S. 2013, *ApJL*, **771**, L45